Improving water-use efficiency of artificial ice reservoirs (Icestupas) through weather-sensitive fountain scheduling strategies

Suryanarayanan Balasubramanian[1,2], Martin Hoelzle[1], and Roger Waser[3]

[1]University of Fribourg, Department of Geosciences, Fribourg, Switzerland
[2]Himalayan Institute of Alternatives, Ladakh, India
[3]University of Applied Sciences and Arts, Luzern, Switzerland

Correspondence: suryanarayanan.balasubramanian@unifr.ch

Abstract.

Artificial Ice Reservoirs (AIRs), often also called - Ice Stupas - are a climate change adaptation strategy developed in the Indian Himalayas (Ladakh). With this technology, otherwise unused stream water is stored in large ice towers in winter. The surplus melt water that is generated in spring is used for satisfying irrigation water demands. Recent studies have shown that during construction of traditional AIRs over 75 % of the water sprayed was lost. Therefore, fountain wastewater production has to be reduced for improving water use efficiency. During the winter of 2021-22, a traditional and an automated AIR were built in Guttannen, Canton of Berne, Switzerland with the main aim of comparing and quantifying the benefits of fountain scheduling. Fountain scheduling was realized through an automation system computing recommended discharge rates using real-time weather input and location metadata. The scheduled fountain produced similar volumes while consuming 87 % less water than the unscheduled fountain. Simulations converting unscheduled fountains to scheduled fountains improved the water use efficiency of several traditional AIRs more than two fold. Overall, these results show that the automated construction strategy can increase the water use efficiency of AIRs without compromising their meltwater production.

1 Introduction

Cryosphere-fed irrigation networks in arid mountain regions are completely dependent on timely availability of meltwater from glaciers, snow and permafrost (Immerzeel et al., 2020; Farhan et al., 2015; Tveiten, 2007). With the accelerated decline of glaciers due to climate change (Nüsser and Baghel, 2016), these regions are experiencing water scarcity particularly during the spring season (Norphel and Tashi, 2015). This seasonal water scarcity makes it essential to provide supplementary irrigation in order to sustain agricultural output and take advantage of the complete growing season (Nüsser and Baghel, 2016; Vincent, 2009).

To cope with this recurrent water scarcity, villagers in the region of Ladakh have developed two types of artificial ice reservoirs (AIRs): ice terraces and ice stupas (see Fig. 1). All these types of ice reservoirs capture water in the autumn and winter, allowing it to freeze, and hold it until spring, when it melts and flows down to fields (IPCC, 2019; Vince, 2009; Clouse et al., 2017; Nüsser et al., 2019). In this way, they retain a previously unused portion of the annual flow and facilitate its use to supplement the decreased flow in the following spring. This study focuses on the form of AIRs locally called as ice stupas.

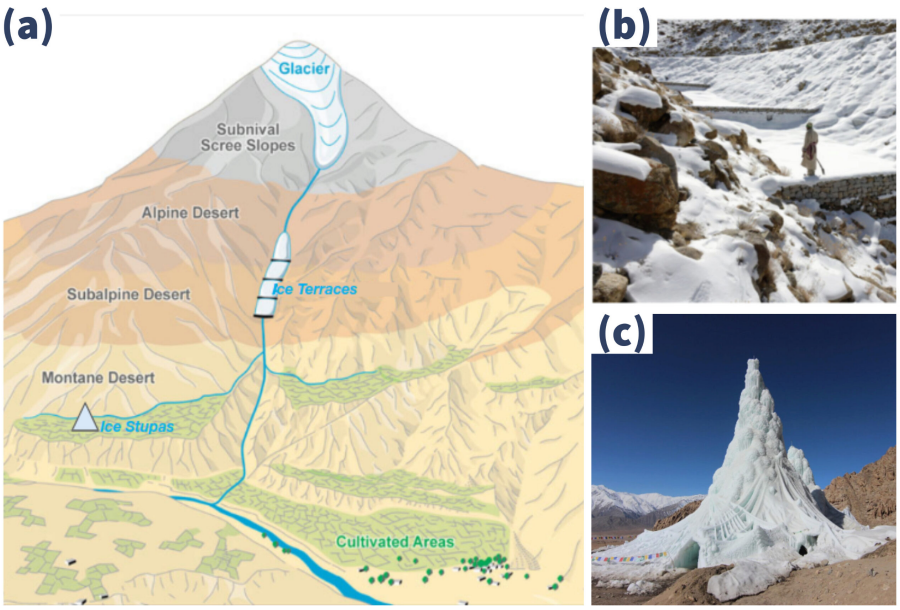

Figure 1. (a) Schematic overview of the position of artificial ice reservoirs. These constructions are located at altitudes between the glaciers and the irrigation networks in the cultivated areas. Ice terraces and ice stupas are located at higher and lower altitudes respectively. Adapted from: Nüsser and Baghel (2016)

Over the past decade, several ice stupas have been built to supplement irrigation water supply of mountain villages in India (Wangchuk, 2020; Palmer, 2022; Aggarwal et al., 2021), Kyrgyzstan (BBC News, 2020) and Chile (Reuters, 2021). These AIRs are traditionally constructed by diverting springs or glacial streams into fountain spray systems via embankments and pipelines.

One of the most common problems with AIR construction systems has to do with fountain scheduling. Fountain scheduling is simply answering the questions of "When do we spray?" and "How long do we spray?". Starting fountain spray too early and/or running a fountain spray too long is considered overwatering. At the very least this practice wastes water. However, overwatering can cause accelerated ice melt if done on a prolonged basis. Likewise, starting fountain spray too late or not running the system for a long enough period of time is considered under watering and can cause reduced ice volumes.

Previous work (Balasubramanian et al., 2022) has shown that traditional construction systems tend to suffer from overwatering. Knowledge of surface freezing rates is important to avoid overwatering. Surface freezing rates can be calculated by means of the full energy balance model developed in Balasubramanian et al. (2022). This model can be forced with either historical weather data or real-time weather data to produce recommended discharge rates.

However, there are several issues that need to be addressed before operating such weather-sensitive fountains. For example, in the case of the Indian AIR, the fountain discharge rate could have been halved since they were always two times higher than the modelled freezing rate (Balasubramanian et al., 2022). However, in practice, reduction of discharge rate would compromise

the maximum ice volume obtained due to reduction in the fountain spray radius and could increase the maintenance cost due to higher risk of fountain freezing events.

An optimum construction strategy, therefore, should first prevent the occurrence of these two events before reducing discharge rates. Spray radius can be maintained if the fountain aperture diameter is lowered with the discharge rate. Fountain freezing events can be prevented if the discharge is not lowered below a minimum threshold.

Recommended discharge rate needs to be sensitive to constraints on the water supply or weather of the construction site. Locations limited by their water supply like in Ladakh, India would prioritize water use efficiency whereas those limited by the favourable weather windows like in Guttannen, Switzerland would prioritize for maximum ice volume. Accordingly, we use two types of model parameter optimizations that prevent underwatering and overwatering to attain higher ice volumes and higher water use efficiency respectively.

However, manually adjusting the fountain discharge rate is not practical due to two reasons. Firstly, this would involve constant adjustments of discharge rates in response to the significant diurnal and seasonal variations of the freezing rates. Secondly, frequent pipeline water drainage is required to avoid water losses. Therefore, operation of weather-sensitive fountains via automation systems is preferred to reduce the maintenance long-term costs.

The present study was performed to compare two AIRs produced using different fountain scheduling strategies but exposed to identical meteorological conditions. The specific objectives of this study is to include the water-use efficiency and maximum ice volume comparison of different fountain scheduling strategies, presentation of the automation system, and examples of its application to the computation of fountain scheduling strategies.

2 Study sites and data

In this study, we use some datasets presented in our previous work (Balasubramanian et al., 2022) along with new datasets. These old datasets record the meteorological conditions and fountain characteristics of AIRs built in Gangles, India (IN21) and Guttannen, Switzerland (CH21) during the winter of 2020-21. In this section, we focus on describing the AIR datasets collected in Guttannen, Switzerland during the winter of 2021-22 (CH22).

The Guttannen site (46.66 °N, 8.29 °E) is situated in the Berne region, Switzerland and has an altitude of 1047 m a.s.l. In the winter (Oct-Apr), mean daily minimum and maximum air temperatures vary between -13 and 15 $°C$. Clear skies are rare, averaging around 7 days during winter. Daily winter precipitation can sometimes be as high as 100 mm. These values are based on 30 years of hourly historical weather data measurements (Meteoblue, 2021). Two AIRs were constructed by the Guttannen Bewegt Association, the University of Fribourg and the Lucerne University of Applied Sciences and Arts during the winters of 2021-22 using a traditional and an automated construction strategy.

The automated and the traditional AIRs were constructed adjacent to each other as shown in Fig. 2. This ensured both AIRs shared the same water source and identical weather conditions. In addition, a webcam guaranteed a continuous survey of the automated AIR.

Figure 2. Automated and traditional AIRs at Guttannen on February 6, 2022. Picture credits: Daniel Bürki

In the traditional strategy, the fountain was operated manually whereas in the automated strategy a programmed automation system controlled the fountain discharge rate during the whole study period using real time weather input and several control parameters, which could be modified via a user interface. Henceforth, we refer to the fountain used in the traditional and automated construction strategy as unscheduled and scheduled fountains respectively.

In the traditional construction strategy, tree branches were laid covering the fountain pipe to initiate and speed up the ice cone formation process. In the automated strategy, only the fountain pipe was placed before the water spray started. The construction of both the AIRs began on 8th December on a snow bed of 13 cm thickness and ended on 12th April. These two dates are denoted as start and expiry dates henceforth.

2.1 Meteorological data

Air temperature, relative humidity, wind speed, pressure, long-wave, short-wave direct and diffuse radiation are required to calculate the surface energy balance of an AIR. The weather data source was an automatic weather station (AWS) located around 20 m away as shown in Fig. 2. Less than 0.4 % of the data was found to be missing and the data gaps were filled by linear interpolation. Hourly ground temperature measurements were also recorded by the AWS to approximate the fountain's water temperature.

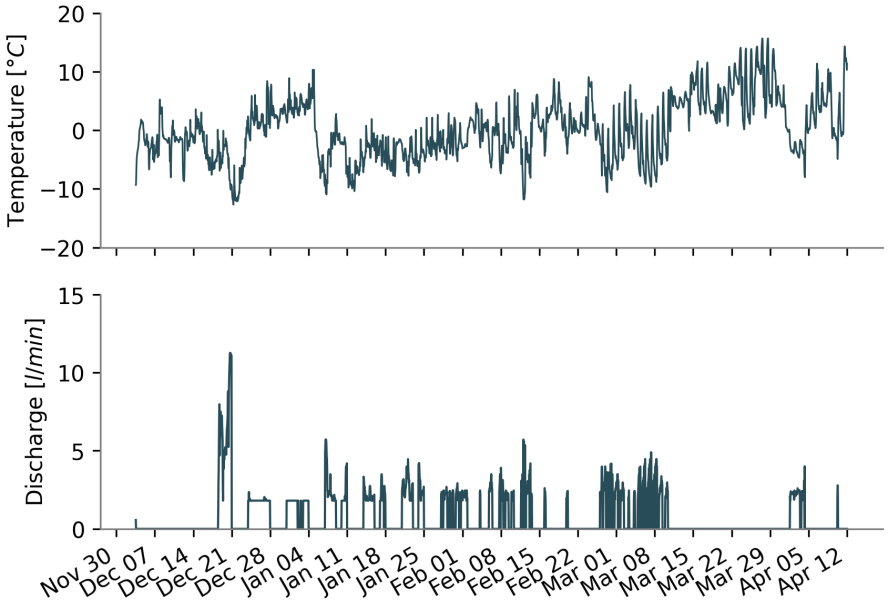

Figure 3. Temperature and discharge measurements at the Guttannen construction site

2.2 Fountain observations

The fountain consists of a pipeline and a nozzle. The pipeline has three attributes, namely : discharge rate (Q), height (h) and water temperature (T_F). Discharge rate represents the discharge rate of the water in the fountain pipeline. Height denotes the height of the fountain pipeline installed. Fountain water temperature is the temperature of water droplets produced by the fountain.

The fountain nozzle has three characteristics, namely : the aperture diameter (dia), the spray radius (r) and pressure loss (P) .The fountain nozzle is assumed to have only one aperture with diameter dia from where water is sprayed. Spray radius denotes the observed ice radius formed from the fountain water droplets. Pressure loss denotes the loss of water head caused due to the fountain nozzle.

Fig. 3 shows how the automation system scheduled the discharge rate based on real-time meteorological conditions. The automation system caused these variations through its control valve which varied between 0 to 100 % depending on the recommended discharge rate. Throughout the study period, the control valve was opened completely (100 %) only once corresponding to the time when the temperature attained its minimum of -13 °C on 20th December. After this event, the control valve was never opened beyond 34 %.

The unscheduled fountain was manually operated to spray all the available discharge until a fountain freezing event interrupted the discharge on 17th February. Unfortunately, no discharge rate measurements were recorded for the unscheduled

Table 1. Summary of the drone surveys

	No.	Date	Volume	Radius	Surface Area
Traditional	1	Dec 23, 2021	17 m^3	2.9 m	47 m^2
	2	Jan 3, 2022	22 m^3	3.4 m	61 m^2
	3	Jan 22, 2022	35 m^3	4 m	79 m^2
	4	Feb 6, 2022	44 m^3	4.2 m	86 m^2
	5	Feb 20, 2022	43 m^3	4.3 m	86 m^2
	6	Mar 19, 2022	33 m^3	4.4 m	84 m^2
	7	Mar 26, 2022	24 m^3	4.3 m	74 m^2
	8	Apr 12, 2022	11 m^3	3.5 m	50 m^2
Automated	1	Dec 23, 2021	35 m^3	4.3 m	73 m^2
	2	Jan 3, 2022	32 m^3	4.4 m	81 m^2
	3	Feb 20, 2022	60 m^3	5.3 m	105 m^2
	4	Mar 19, 2022	28 m^3	3.7 m	57 m^2
	5	Mar 26, 2022	19 m^3	3.7 m	53 m^2
	6	Apr 12, 2022	7 m^3	2.5 m	53 m^2

fountain. Therefore, this dataset was estimated from the discharge rate measurements and characteristics of the scheduled fountain.

The height was also increased in steps of 1 meter for both the fountains. This caused variations in the corresponding discharge rate. For the scheduled fountain, the construction began with a height of 3 m with an increase to 4 m on 23rd December. This fountain height increase reduced its maximum discharge from 13 l/min to 11 l/min. For the unscheduled fountain, the construction began with a height of 3.7 m and then this was increased two times on 23rd December and 12th February.

The water temperature of both the fountains were estimated from the AWS ground temperature dataset.

The spray radius was estimated for both the fountains from several drone flights. Ice radius measurements of drone flights which observed either an increase in AIR circumference or volume were averaged to determine the fountain's spray radius.

2.3 Drone surveys

Several photogrammetric surveys were conducted on the traditional and the automated AIRs. The details of these surveys and the methodology used to produce the corresponding outputs are explained in Balasubramanian et al. (2022). The digital elevation models (DEMs) generated from the obtained imagery were analysed to document the spray radius, the surface area and the volume of the ice structures. The number of drone surveys conducted for the traditional and the automated AIRs were 8 and 6, respectively (see Table 1).

Table 2. Assumptions for the parametrisation introduced to simplify the model.

Estimation of	Symbol	IVOM	WEOM
Slope	s_{cone}	1	0
Albedo	α	α_{snow}	α_{ice}
Cloudiness	cld	0	1

3 Methods

3.1 Determination of recommended discharge rate

Recommended discharge rate of the automation system depend upon whether the construction location is constrained by the available water supply or the duration of favourable weather windows for fountain operation. If the respective location has limited water supply then the fountain scheduling strategy should be optimised for water-use efficiency . But if the location is limited by the time period when the fountain can function then the scheduling strategy should be optimised for ice volumes.

Accordingly, we introduce two kinds of model forcing assumptions corresponding to the ice volume and water-use efficiency objective for the following three model variables: (a) slope , (b) albedo and (c) cloudiness. The slope variable increases the shortwave radiation and sensible heat impact. The albedo variable decreases the shortwave radiation impact. The cloudiness variable increases both the shortwave and the longwave radiation impact. Therefore, increase of slope and cloudiness variable increases melting energy and increase of albedo variable increases freezing energy. Assumptions used for the ice volume and water-use efficiency objectives overestimate and underestimate the freezing rate of the AIR respectively. Correspondingly, we associate the upper and lower bounds of these variables as shown in Table 2. These two kinds of models will be referred to as ice volume optimised model (IVOM) and water-use efficiency optimised model (WEOM) respectively.

We apply the assumptions described in Table 2 on the one-dimensional description of energy fluxes as used in Balasubramanian et al. (2022) to obtain the rate of change of AIR ice mass as follows:

$$\frac{\Delta M_{ice}}{\Delta t} = \left(\frac{q_{SW} + q_{LW} + q_S + q_F + q_R + q_G - q_T}{L_F} + \frac{q_L}{L_V}\right) \cdot A_{cone} \tag{1}$$

Upward and downward fluxes relative to the ice surface are positive and negative, respectively. The first term represents the mass change rate due to freezing of the fountain water and melting of the ice. q_{SW} is the net short-wave radiation; q_{LW} is the net long-wave radiation; q_L and q_S are the turbulent latent and sensible heat fluxes; q_F is the fountain discharge heat flux; q_R is the rain water heat flux; q_G is the ground heat flux; q_T is the temperature heat flux and A_{cone} is the area of the AIR surface. The derivation of these individual terms for the IVOM and WEOM model versions are discussed in the Appendix C.

Equation 1 is implemented in the automation system through a user interface that enables input of the spray radius, altitude, latitude and longitude of the construction location. Once switched on, the automation system regulates the fountain discharge

rate based on the recommended discharge rate. Further details about how the automation system functions can be found in Appendix A.

3.2 Model updates

The model was made more sensitive to fountain discharge rate feedback for comparing the volume evolution of the automated and traditional AIRs. These updates are explained in detail in Appendix B.

3.3 Calibration and Validation

The model parameters were calibrated to the median values of the ranges presented in Appendix Table A1.

We performed the validation of the model on the traditional and automated AIRs by evaluating the root mean squared error (RMSE) between volume estimates and measurements.

The performance of the IVOM and WEOM versions of the physical model was assessed by comparing correlation of its discharge rate estimates with the validated freezing rate of calibrated model.

3.4 Fountain characteristics

The aperture configuration of the scheduled and unscheduled fountains were far too complex to enable a direct comparison (see Fig.). To circumvent this, both the fountain designs were approximated to a simple fountain design with just one aperture (see Fig.). Then the corresponding aperture diameter (dia) of this simple fountain was chosen so that it validates the observations recorded for the different fountains.

The fountain's height (h), aperture diameter (dia) and pressure loss (P) were related to its discharge rate (Q) through the Bernoulli equation :

$$P_i + \rho_{water} \cdot g \cdot h_i + 1/2 \cdot \rho_{water} \cdot v_i^2 = P_f + \rho_{water} \cdot g \cdot h_f + 1/2 \cdot \rho_{water} \cdot v_f^2 \tag{2}$$

where ρ_{water} is the density of water and v is the velocity of the fountain water droplets. The subscripts i and f refer to the initial and final states of the system. v can be determined from the discharge rate Q through the mass conservation equation as

$$v = 4 \cdot Q/(\pi \cdot dia^2) \tag{3}$$

Combining the Eqns. 2 and 3, we get the final discharge Q_f after a height change from h_i to h_f to be:

$$Q_f = \sqrt{Q_i^2 + 2 \cdot g \cdot (h_i - h_f) \cdot (\pi \cdot dia^2/4)^2} \tag{4}$$

Assuming that the water droplets have diameter equal to the fountain apertutre diameter and follow projectile motion starting from a fountain height h with a launch angle $\theta = 45°$, we get the following equation for the spray radius r:

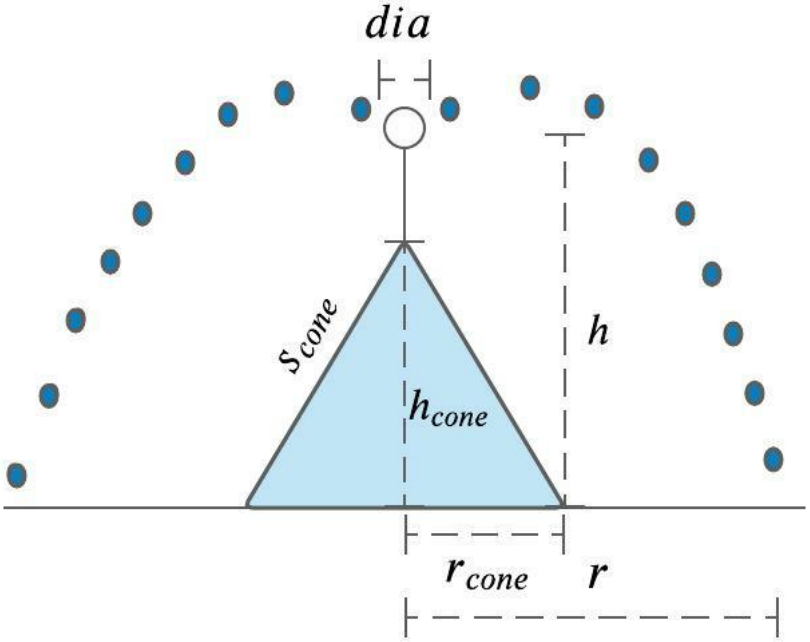

Figure 4. Shape variables and fountain characteristics of the AIR. r_{cone} is the radius, h_{cone} is the height and s_{cone} is the slope of the AIR ice cone. r is the spray radius, dia is the aperture diameter and h is the fountain height

$$r = \frac{v \cdot (v + \sqrt{v^2 + 4hg})}{2g} \tag{5}$$

4 Results

4.1 Estimation of fountain characteristics

The influence of the fountain height increase event on the maximum discharge rate was used to determine the fountain nozzle's aperture diameter. The maximum discharge rate of the scheduled fountain reduced from Q_i = 13 l/min to Q_f = 11 l/min when the fountain height was raised from h_i = 3 m to h_f = 4 m. Inputting the corresponding values in Eqn. 2, we get the estimated fountain aperture diameter (dia) to be around 5 mm.

The change in discharge rate observed upon removal of the fountain nozzle was used to determine the fountain pressure loss. When the fountain nozzle was removed, the maximum discharge rate of the fountain was observed to increase from Q_i = 11 l/min to Q_f = 27 l/min. Using the fountain aperture diameter $d_i = 5mm$, the pipeline diameter $d_f = 19mm$, $P_f = 0$ and

$h_i = h_f$ in Eqn. 2 we estimate the pressure loss occurring due to the fountain nozzle to be equivalent to 4.3 meters of water head.

4.2 Unscheduled discharge rate estimation

The pressure loss of unscheduled fountain was determined by assuming a linear relationship of pressure loss with aperture diameter. We use two observations to determine this linear relationship, namely, that the pressure loss of the fountain was zero with a diameter of 19 mm (fountain removal event) and that the scheduled fountain had a pressure loss of 4.3 m with an aperture diameter 5 mm. We estimate that for a constant height the pressure decreases by 18 mm for every 1 mm increase in aperture diameter (see Fig. 5 (a)).

The fountain freezing event observation was used to determine the unscheduled fountain nozzle's aperture diameter. The unscheduled fountain had a fountain freezing event at height 5.7 m. We assume that its discharge rate was close to zero during this event. The aperture diameter with the fountain freezing height closest to 5.7 m is 7 mm according to Eqn. 2 as shown in Fig. 5 (b) . The corresponding pressure loss of a fountain with 7 mm diameter is 3.7 m as shown in Fig. 5 (a).

Fig. 5 (c) shows the unscheduled discharge rate estimated for the study period. The temporal variation in the discharge rate is caused due to the the two height increase events on 23rd Dec and 12th February that increased the height from 3.7 to 5.7 m respectively.

4.3 Scheduled discharge rate simulations

We found that the WEOM and IVOM model versions estimated the freezing rate of the unscheduled fountain with a correlation around 0.6 and a RMSE less than 0.6 l/min and 1.6 l/min respectively. The IVOM scheduled fountain overestimated the freezing rate 44 % of the construction duration whereas the WEOM scheduled fountain underestimated the freezing rate 67 % of the construction duration. Therefore, the IVOM and WEOM model forcings were successful in prioritizing the maximum ice volume and water use efficiency metrics respectively.

4.4 Model validation

The volume estimation for the automated and traditional AIR had an RMSE of 13 m^3 and 5 m^3 with the drone volume observations, respectively. This RMSE error is within 20 % and 11 % of the maximum volume of the automated and the traditional AIR respectively. The estimated and measured AIR volumes are shown in Fig. 6.

4.5 Comparison of AIR construction strategies

Table 3 shows how the different fountain scheduling strategies influence the mass and energy balance of the respective AIR. The difference between the fountain discharge input and fountain wastewater output of the unscheduled and scheduled fountains was around an order of magnitude.

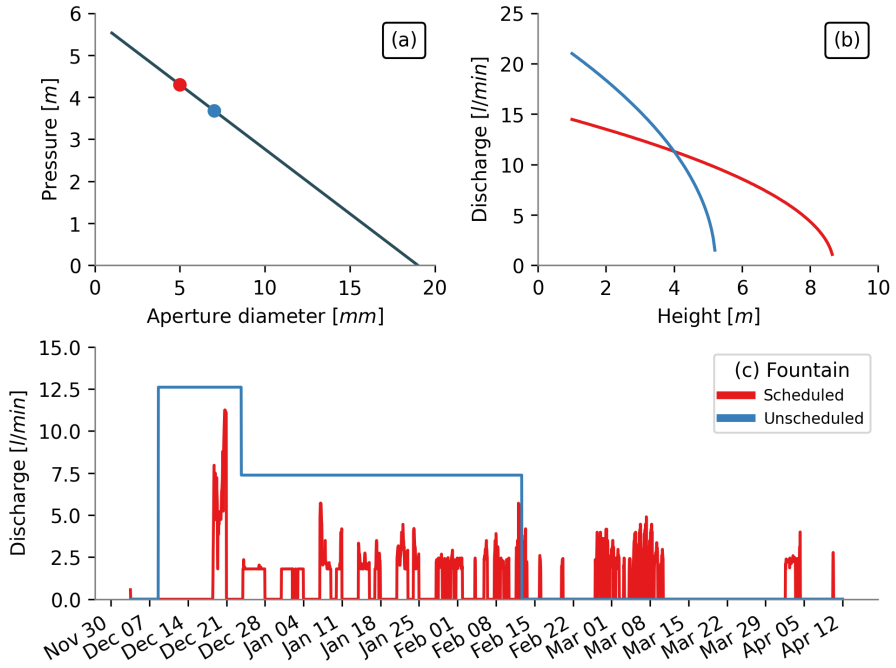

Figure 5. (a) Pressure loss as a linear function of aperture diameter for a constant fountain height and discharge rate. The corresponding values for the scheduled and unscheduled fountains are highlighted as red and blue dots respectively. (b) Discharge as a function of height for the scheduled (red curve) and the unscheduled (blue curve) fountain for a constant aperture diameter and pressure loss. (c) Discharge measured for the scheduled fountain (red curve) and estimated for the unscheduled fountain (blue curve) during the study period.

During fountain spray, the AIR surface (a) albedo dampens to ice albedo and (b) absorbs the heat energy of the fountain water droplets. These two processes are the cause of the difference in the mass and energy balance distribution shown in Table 3. The temporal variation of the magnitude of these processes are shown in Fig. 7.

The overall impact of the radiation fluxes (long-wave and short-wave) and the turbulent fluxes (sensible and latent) on the freezing and melting energies is determined from their respective energy turnover. The energy turnover is calculated as the sum of energy fluxes in absolute values (see Table 3).

There is a considerable difference in the contribution of the shortwave radiation due to the effect of process (a). Even though the unscheduled fountain was active for a much longer duration, the frequent snowfall events counteracted the albedo feedback of its fountain discharge. However, the albedo of the automated AIR was significantly impacted by late fountain spray events particularly in the month of March and April as shown in Fig. 7.

Similarly, the fountain discharge heat flux for the traditional AIR was enhanced due to process (b). The higher discharge quantity of the unscheduled fountains and its longer duration were responsible for the 10 fold increase in its fountain discharge heat flux.

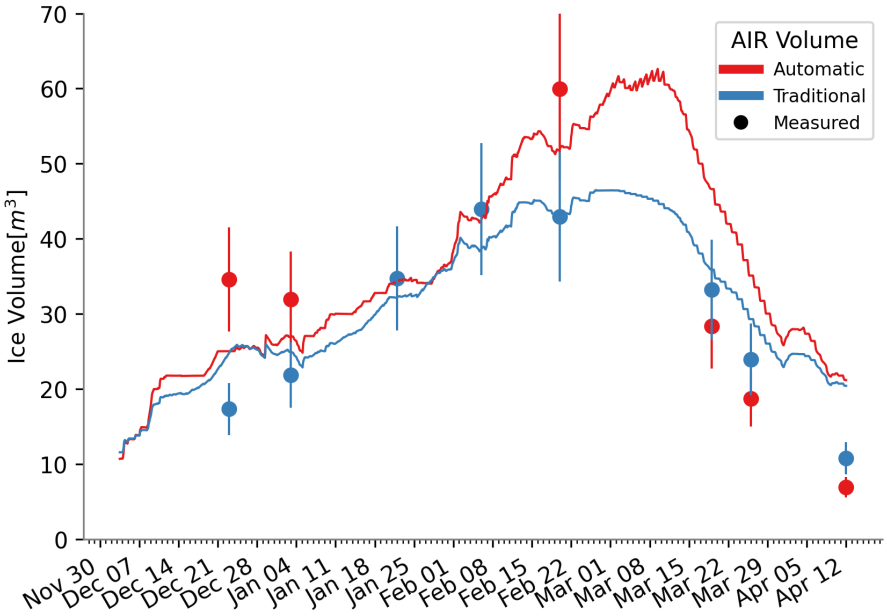

Figure 6. Volume validation of the scheduled and unscheduled fountain construction strategies.

5 Discussion

5.1 Benefits of scheduling fountains

The difference in water-use efficiency and maximum volume between unscheduled and scheduled fountains in the two locations across two winters are presented in Fig. 9. Four experimental values (highlighted by circles) are shown together with five simulated values (highlighted by squares). The experimental values were taken from the IN21 and CH21 AIRs studied in Balasubramanian et al. (2022) and the CH22 AIR presented in this study.

The water-use efficiency of all the unscheduled fountains are below 20 %. In general, the water-use efficiency increases more than two fold when the IVOM or WEOM fountain is used in both the locations.

There is also a considerable difference between the outputs of WEOM and IVOM fountains for each AIR. For CH21 AIR, WEOM fountain does not yield any ice formation whereas IVOM fountain succeeds in increasing the water-use efficiency three fold. For CH22 AIR, both experimental and simulated values of IVOM fountains yield an increase in water-use efficiency from 4 % to around 31 %. The WEOM fountain succeeded in increasing the water-use efficiency up to 2 times higher than the IVOM fountain.

For the Swiss location, scheduled fountains yield better water-use efficiency but do not alter the maximum volume obtained significantly.

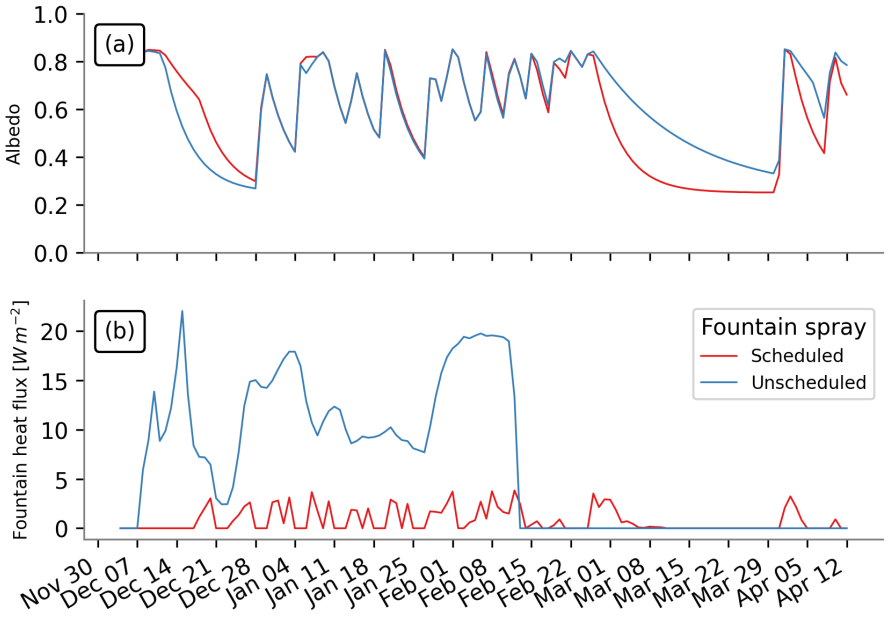

Figure 7. (a) Surface albedo and (b) fountain discharge heat flux showed significant variations between the two AIRS due to the differences in their discharge rates.

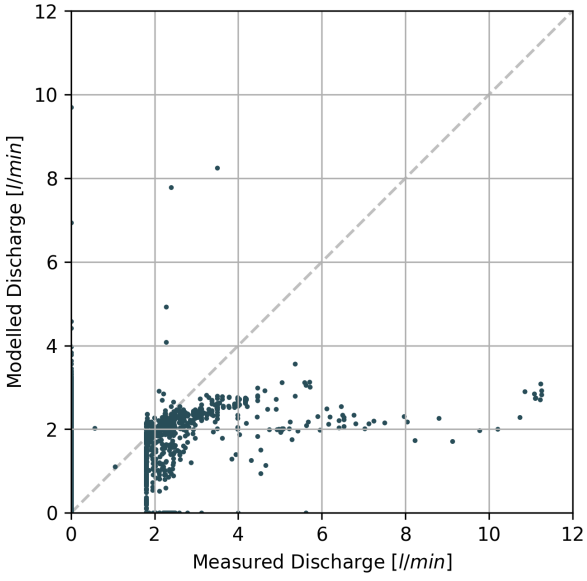

Figure 8. Comparison of the discharge rate measured by the automation system and the discharge rate simulated by the IVOM model.

Table 3. Summary of the mass balance, energy balance, fountain and AIR characteristics estimated at the end of the respective simulation duration for the automated and the traditional AIRs

	Name	Symbol	Traditional	Automated	Units
Input	Fountain discharge	M_F	8.2×10^5	1.4×10^5	kg
	Snowfall	M_{ppt}	1.1×10^4	1.5×10^4	kg
	Deposition	M_{dep}	9.4×10^2	1.2×10^3	kg
Output	Meltwater	M_{water}	2.9×10^4	4.2×10^4	kg
	Ice	M_{ice}	1.3×10^4	1.3×10^4	kg
	Sublimation	M_{sub}	2.6×10^3	3.0×10^3	kg
	Fountain wastewater	M_{waste}	8.0×10^5	1.1×10^5	kg
Energy Flux	Shortwave radiation	q_{SW}	29	39	%
	Longwave radiation	q_{LW}	35	34	%
	Sensible heat	q_S	8	8	%
	Latent heat	q_L	17	17	%
	Fountain discharge heat	q_F	10	1	%
	Rain heat	q_R	0	0	%
	Ground heat	q_G	1	2	%
Fountain	Spray Radius	r	4.8	4.1	m
	Aperture Diameter	dia	5	7	mm
	Pressure Loss	P	4.3	3.7	m
	Minimum discharge rate	Q_{min}	2	N.A.	l/min
AIR	Maximum AIR Volume		47	63	m^3
	Water Use Efficiency		4	31	%

For the Indian location, the two kinds of scheduled fountains yield significantly different results when compared to the unscheduled fountain. The IVOM fountain achieved a 1.5 fold increase in the maximum volume and a 2 fold increase in the water-use efficiency. The WEOM fountain had a water-use efficiency of 73 % but its maximum volume was lower than the unscheduled fountain.

The discharge duration and the max discharge rate of the three IN21 fountains were responsible for these different results (see Fig. 9 (b)). The max discharge rate of the unscheduled fountain was more than twice that of scheduled fountains resulting in a high water loss. Fountain freezing events caused frequent interruptions in the unscheduled discharge rate (see Fig. 9 (b)). Therefore, the discharge duration of the unscheduled fountain was much lower resulting in lower ice volumes. The WEOM fountain underestimated the freezing rate during the construction period and therefore produced much lower ice volumes compared to the IVOM fountain.

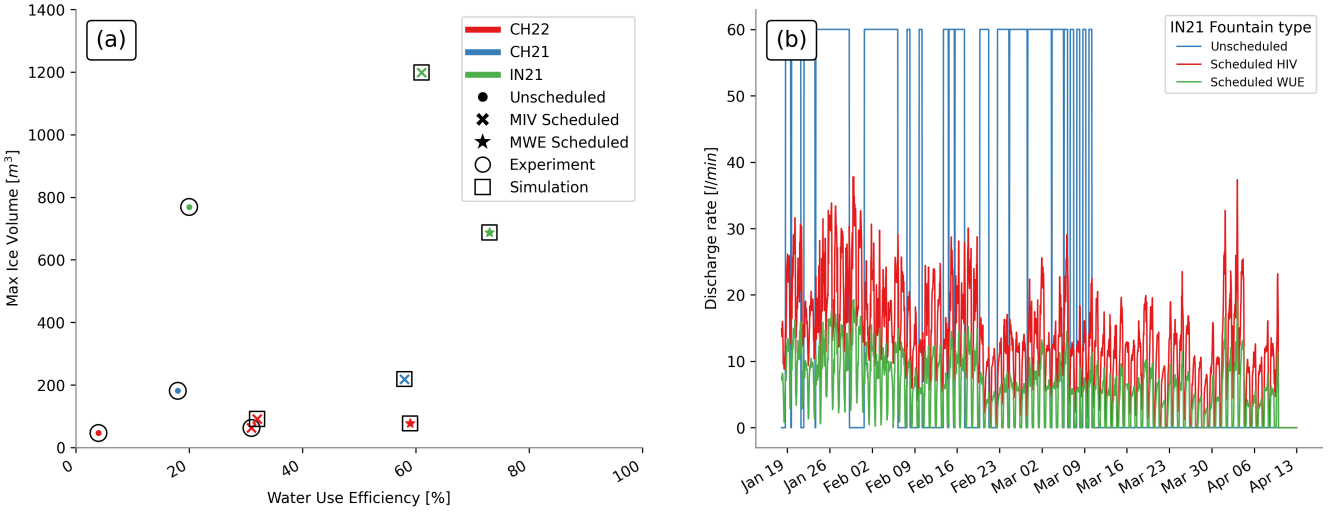

Figure 9. (a) The maximum volumes and water-use efficiency estimated for AIRs constructed in different locations (represented by colours) with different fountain scheduling strategies (represented by symbols). Experimental values are highlighted by circles and simulated values are highlighted by squares. (b) Comparison of the unscheduled and scheduled fountain's discharge rates at the IN21 location.

5.2 Challenges of scheduling fountains

5.2.1 Determination of minimum discharge rate

The value of minimum discharge rate determines the duration of the favourable weather windows and the risk of fountain freezing events. Therefore, its accurate quantification is critical. The risk of a fountain freezing event is inversely proportional to the spray radius. Therefore, minimum discharge rate can be determined based on the minimum fountain spray radius desired. In the case of the CH22 experiment, the minimum discharge rate of 2 l/min corresponded to a spray radius of around 1 m.

5.2.2 Determination of fountain spray radius

To schedule fountains, one needs to estimate their spray radius accurately since the recommended discharge rate is proportional to the square of the spray radius used. Manual measurements of the fountain spray revealed a maximum spray radius of just 3 m but drone measurements reveal a fountain spray radius of 4.8 m for the scheduled fountain. This discrepancy could be caused by both wind drift of water droplets and refreezing events across the boundary of the AIR.

6 Conclusions

In this paper, an automated AIR construction strategy is presented and compared with a traditional strategy using data collected in Guttannen, Switzerland and Gangles, India.

The main purpose of this study was to quantify the influence of different fountain designs and weather-sensitive scheduling strategies on the water use efficiency and volumes of AIRs exposed to identical weather conditions. We found that overwatering not just increased the fountain wastewater production but also enhanced the melting rate of AIRs, mainly due to its surface albedo and fountain heat flux feedbacks. Furthermore, the freezing rate of the scheduled fountain was also enhanced by its lower aperture diameter, which contributed to its higher spray radius. As a consequence, the automated AIR was able to reduce its water consumption by 87 % and increase its maximum volume by 34% compared to the traditional AIR.

Two different model forcings sensitive to the limited weather windows or water supply of a new location were used to produce two types of recommended discharge rates favouring higher volumes and better water use efficiencies, respectively. Nevertheless, these models were able to capture more than 44 % of the freezing rate variations produced by the full energy balance model. Simulations comparing scheduled and unscheduled fountains show that up to a two fold increase in water use efficiency is possible without compromising on meltwater production.

Fountain design is an important area where improvement is necessary since it can be used to increase AIR ice volumes. If the scheduled fountain of the CH22 experiment was replaced with a fountain with a lower pressure loss but with the same aperture diameter, the automated AIR would have produced more meltwater. Future research must be devoted to engineer such fountains that create larger AIRs effortlessly and efficiently.

Appendix A: Automation system

The automation hardware consists of an AWS, flowmeter, control valve, drain valves, air valves, fountain, pipeline and a logger. The logger feeds the AWS data to the automation software and informs the recommended discharge rate to the flowmeter. The flowmeter adjusts the control valve to match the recommendation. In case a termination criteria is valid, the drain and air valves allow the removal of water from the pipeline and entry of air in the pipeline respectively.

The recommended discharge rate is equal to the ice mass change rate. However, certain termination criteria override the discharge rate recommendation and drain the pipeline to prevent water loss or fountain freezing events, namely:

- High water loss is assumed if wind speed is greater than the user-defined critical wind speed.
- High risk of fountain freezing event is assumed if $\frac{\Delta M_{ice}}{\Delta t}$ is lower than the user-defined minimum fountain discharge rate.
- Fountain freezing events are assumed if measured discharge rate is zero for at least 20 seconds and the pipeline is drained as a consequence.
- Pipeline leakage is assumed if measured discharge rate is greater than the user-defined maximum fountain discharge rate.

Appendix B: Model updates

In the previous version of the model (Balasubramanian et al., 2022), the fountain water temperature (T_F) was estimated as a constant parameter. However, in reality, this is a poor approximation. This is because the fountain water temperature and source water temperature differ due to the temperature change caused by transit from the source to the AIR surface. Therefore, we instead use measured hourly ground temperature measurements to approximate water temperature for both the AIRs.

In the previous version of the model (Balasubramanian et al., 2022), fountain discharge events were reset from surface albedo to ice albedo. However, this assumption limits the accuracy of the model, especially, for the automated AIR where several fountain discharge events of short durations occur. Therefore, we assumed that discharge events instead reduce the albedo decay rate (τ) by a factor of $\frac{\alpha_{ice}}{\alpha_{snow}}$.

Additionally, both the AIRs experienced many precipitation events. Therefore, it was no longer accurate to assume AIR density (ρ_{cone}) to be equal to ice density. We instead parameterised AIR density ρ_{cone} as follows:

$$\rho_{cone} = \frac{M_F + M_{dep} + M_{ppt}}{(M_F + M_{dep})/\rho_{ice} + M_{ppt}/\rho_{snow}} \tag{B1}$$

where M_F is the cumulative mass of the fountain discharge; M_{ppt} is the cumulative precipitation; M_{dep} is the cumulative accumulation through water vapour deposition; ρ_{ice} is the ice density (917 $kg\,m^{-3}$) and ρ_{snow} is the density of wet snow (300 $kg\,m^{-3}$) taken from Cuffey and Paterson (2010) .

Rain events were not considered in the previous version of the model but they occur in our experiment. The influence of rain events on the albedo and the energy balance was assumed to be similar to that of discharge events. However, the water temperature of a rain event was assumed to be equal to the air temperature. Accordingly, the heat flux generated due to a rain event was equal to:

$$q_R = \frac{\Delta M_{ppt} \cdot c_{water} \cdot T_a}{\Delta t \cdot A_{cone}} \tag{B2}$$

Appendix C: Model forcing based on water-use efficiency and maximum volume objectives

The model complexity and data requirement (Balasubramanian et al., 2022) were reduced through assumptions that optimise for the ice volume or the water-use efficiency objectives. We define the freezing rate and melting rate as the positive and negative mass change rate, respectively. Assumptions are chosen, based on whether they overestimate/underestimate the freezing rate. HIV objective requires freezing rate to be overestimated whereas water-use efficiency objective requires freezing rate to be underestimated. We describe these two kinds of assumptions applied on each of the energy balance components below:

C1 Surface Area A_{cone} assumptions

Determination of the surface area during the accumulation period is achieved by assuming a constant ice cone radius equal to the fountain spray radius. The surface area scales the freezing rate of the AIR. Hence, for the HIV objective, we assume the maximum possible slope of 1 for the ice cone or in other words $h_{cone} = r_F$. Therefore, area is estimated as:

$$A_{cone} = \sqrt{2} \cdot \pi \cdot r_F^2 \tag{C1}$$

Similarly, for the water-use efficiency objective, the area of the conical AIR is approximated to the area of its circular base. Therefore, area is estimated as:

$$A_{cone} = \pi \cdot r_F^2 \tag{C2}$$

C2 Net shortwave radiation q_{SW} assumptions

The net shortwave radiation q_{SW} is computed as follows:

$$q_{SW} = (1 - \alpha) \cdot (SW_{direct} \cdot f_{cone} + SW_{diffuse}) \tag{C3}$$

where α is the albedo value ; SW_{direct} is the direct shortwave radiation; $SW_{diffuse}$ is the diffuse shortwave radiation and f_{cone} is the solar area fraction.

The data requirement was reduced by estimating the global shortwave radiation and pressure directly using the location's coordinates and altitude through the solar radiation model described in Holmgren et al. (2018). The algorithm used to estimate the clear-sky global radiation is described in Ineichen (2008).

The diffuse and direct shortwave radiation is determined using the estimated global solar radiation as follows:

$$\begin{aligned} SW_{diffuse} &= cld \cdot SW_{global} \\ SW_{direct} &= (1 - cld) \cdot SW_{global} \end{aligned} \tag{C4}$$

where cld is the cloudiness factor. cld is assumed to be 1 and 0 for the water-use efficiency and ice volume objective respectively.

We ignore the variations in the albedo and assume it to be equal to snow albedo and ice albedo for the ice volume and water-use efficiency objective, respectively.

The solar area fraction f_{cone} of the ice structure exposed to the direct shortwave radiation depends on the shape considered. It is computed as

$$f_{cone} = \frac{(0.5 \cdot r_{cone} \cdot h_{cone}) \cdot cos\theta_{sun} + (\pi \cdot (r_{cone})^2/2) \cdot sin\theta_{sun}}{\pi \cdot r_{cone} \cdot ((r_{cone})^2 + (h_{cone})^2)^{1/2}} \tag{C5}$$

For the ice volume objective, since we assume the slope of the cone to be 1, f_{cone} is determined as follows:

$$f_{cone} = \frac{cos\theta_{sun} + \pi \cdot sin\theta_{sun}}{2\sqrt{2} \cdot \pi} \tag{C6}$$

Similarly, for the water-use efficiency objective, since we assume the slope of the cone to be negligible, we get:

$$f_{cone} = \frac{sin\theta_{sun}}{2} \tag{C7}$$

C3 Net Longwave radiation q_{LW} assumptions

We assume $T_{ice} = 0°C$ in order to determine outgoing longwave radiation. Since it is challenging to constrain the minimum ice temperature, we maintain this assumption for both our objectives. However, in order to estimate atmospheric emissivity, we again assume cld to be 1 and 0 for the water-use efficiency and ice volume objective respectively.

C4 Turbulent fluxes assumptions

Turbulent fluxes estimation depend on the slope of the cone through the μ_{cone} parameter. As suggested by Oerlemans et al. (2021), we estimated this parameter as follows:

$$\mu_{cone} = 1 + s_{cone}/2 \tag{C8}$$

Hence, the μ_{cone} parameter takes values of 1.5 and 1 for the ice volume and water-use efficiency objective respectively. Since turbulent fluxes impact both the freezing and the melting rates, this assumption may not favor the corresponding objectives for certain sites.

Table A1. Free parameters in the model categorised as constant, model hyperparameters and weather parameters with their respective values/ranges.

Constant Parameters	**Symbol**	**Value**	**Unit**	**References**
Van Karman constant	κ	0.4	dimensionless	Cuffey and Paterson (2010)
Stefan Boltzmann constant	σ	5.67×10^{-8}	$W\,m^{-2}\,K^{-4}$	Cuffey and Paterson (2010)
Air pressure at sea level	$p_{0,a}$	1013	hPa	Mölg and Hardy (2004)
Density of water	ρ_w	1000	$kg\,m^{-3}$	Cuffey and Paterson (2010)
Density of ice	ρ_{ice}	917	$kg\,m^{-3}$	Cuffey and Paterson (2010)
Density of air	ρ_a	1.29	$kg\,m^{-3}$	Mölg and Hardy (2004)
Specific heat of water	c_w	4186	$J\,kg^{-1}\,^{\circ}C^{-1}$	Cuffey and Paterson (2010)
Specific heat of ice	c_{ice}	2097	$J\,kg^{-1}\,^{\circ}C^{-1}$	Cuffey and Paterson (2010)
Specific heat of air	c_a	1010	$J\,kg^{-1}\,^{\circ}C^{-1}$	Mölg and Hardy (2004)
Thermal conductivity of ice	k_{ice}	2.123	$W\,m^{-1}\,K^{-1}$	Bonales et al. (2017)
Latent Heat of Sublimation	L_s	2.848×10^6	$J\,kg^{-1}$	Cuffey and Paterson (2010)
Latent Heat of Fusion	L_f	3.34×10^5	$J\,kg^{-1}$	Cuffey and Paterson (2010)
Gravitational acceleration	g	9.81	$m\,s^{-2}$	Cuffey and Paterson (2010)
Weather station height	h_{AWS}	2	m	assumed
Model timestep	Δt	3600	s	assumed
Model Hyperparameters	**Symbol**	**Range**	**Unit**	**References**
Surface layer thickness	Δx	$[1 \times 10^{-2}, 1 \times 10^{-1}]$	m	assumed
Weather Parameters	**Symbol**	**Range**	**Unit**	**References**
Ice Emissivity	ϵ_{ice}	$[0.95, 0.99]$	dimensionless	Hori et al. (2006)
Surface Roughness	z_0	$[1 \times 10^{-3}, 5 \times 10^{-3}]$	m	Brock et al. (2006)
Ice Albedo	α_{ice}	$[0.15, 0.35]$	dimensionless	Steiner et al. (2015); Zolles et al. (2019)
Snow Albedo	α_{snow}	$[0.8, 0.9]$	dimensionless	Zolles et al. (2019)
Precipitation Temperature threshold	T_{ppt}	$[0, 2]$	$^{\circ}C$	ShiChang et al. (2010)
Albedo Decay Rate	τ	$[10, 22]$	$days$	Schmidt et al. (2017); Oerlemans and Knap (1998)

References

Aggarwal, A., Frey, H., McDowell, G., Drenkhan, F., Nüsser, M., Racoviteanu, A., and Hoelzle, M.: Adaptation to Climate Change Induced Water Stress in Major Glacierized Mountain Regions, Climate and Development, 0, 1–13, https://doi.org/10.1080/17565529.2021.1971059, 2021.

Balasubramanian, S., Hoelzle, M., Lehning, M., Bolibar, J., Wangchuk, S., Oerlemans, J., and Keller, F.: Influence of Meteorological Conditions on Artificial Ice Reservoir (Icestupa) Evolution, Frontiers in Earth Science, 9, 771 342, https://doi.org/10.3389/feart.2021.771342, 2022.

BBC News: Bright Artificial Glacier in Naryn - BBC Kyrgyz, https://www.youtube.com/watch?v=TpeSQf75bFQ, 2020.

Bonales, L. J., Rodriguez, A. C., and Sanz, P. D.: Thermal Conductivity of Ice Prepared under Different Conditions, International Journal of Food Properties, 20, 610–619, https://doi.org/10.1080/10942912.2017.1306551, 2017.

Brock, B. W., Willis, I. C., and Sharp, M. J.: Measurement and Parameterization of Aerodynamic Roughness Length Variations at Haut Glacier d'Arolla, Switzerland, Journal of Glaciology, 52, 281–297, https://doi.org/10.3189/172756506781828746, 2006.

Clouse, C., Anderson, N., and Shippling, T.: Ladakh's Artificial Glaciers: Climate-Adaptive Design for Water Scarcity, Climate and Development, 9, 428–438, https://doi.org/10.1080/17565529.2016.1167664, 2017.

Cuffey, K. M. and Paterson, W. S. B.: The Physics Of Glaciers, Elsevier, 2010.

Farhan, S. B., Zhang, Y., Ma, Y., Guo, Y., and Ma, N.: Hydrological Regimes under the Conjunction of Westerly and Monsoon Climates: A Case Investigation in the Astore Basin, Northwestern Himalaya, Climate Dynamics, 44, 3015–3032, https://doi.org/10.1007/s00382-014-2409-9, 2015.

Holmgren, W. F., Hansen, C. W., and Mikofski, M. A.: Pvlib Python: A Python Package for Modeling Solar Energy Systems, Journal of Open Source Software, 3, 884, https://doi.org/10.21105/joss.00884, 2018.

Hori, M., Aoki, T., Tanikawa, T., Motoyoshi, H., Hachikubo, A., Sugiura, K., Yasunari, T. J., Eide, H., Storvold, R., Nakajima, Y., and Takahashi, F.: In-Situ Measured Spectral Directional Emissivity of Snow and Ice in the 8–14 Mm Atmospheric Window, Remote Sensing of Environment, 100, 486–502, https://doi.org/10.1016/j.rse.2005.11.001, 2006.

Immerzeel, W. W., Lutz, A. F., Andrade, M., Bahl, A., Biemans, H., Bolch, T., Hyde, S., Brumby, S., Davies, B. J., Elmore, A. C., Emmer, A., Feng, M., Fernández, A., Haritashya, U., Kargel, J. S., Koppes, M., Kraaijenbrink, P. D. A., Kulkarni, A. V., Mayewski, P. A., Nepal, S., Pacheco, P., Painter, T. H., Pellicciotti, F., Rajaram, H., Rupper, S., Sinisalo, A., Shrestha, A. B., Viviroli, D., Wada, Y., Xiao, C., Yao, T., and Baillie, J. E. M.: Importance and Vulnerability of the World's Water Towers, Nature, 577, 364–369, https://doi.org/10.1038/s41586-019-1822-y, 2020.

Ineichen, P.: A Broadband Simplified Version of the Solis Clear Sky Model, Solar Energy, 82, 758–762, https://doi.org/10.1016/j.solener.2008.02.009, 2008.

IPCC: Chapter 2: High Mountain Areas — Special Report on the Ocean and Cryosphere in a Changing Climate, IPCC Special Report on the Ocean and Cryosphere in a Changing Climate, 2019.

Meteoblue: Climate Guttannen, https://www.meteoblue.com/en/weather/historyclimate/climatemodelled/guttannen_switzerland_2660433, 2021.

Mölg, T. and Hardy, D. R.: Ablation and Associated Energy Balance of a Horizontal Glacier Surface on Kilimanjaro, J. Geophys. Res.-Atmos., 109, 1–13, https://doi.org/10.1029/2003JD004338, 2004.

Norphel, C. and Tashi, P.: Snow Water Harvesting in the Cold Desert in Ladakh: An Introduction to Artificial Glacier, in: Mountain Hazards and Disaster Risk Reduction, edited by Nibanupudi, H. K. and Shaw, R., Disaster Risk Reduction, pp. 199–210, Springer Japan, Tokyo, https://doi.org/10.1007/978-4-431-55242-0_11, 2015.

Nüsser, M. and Baghel, R.: Local Knowledge and Global Concerns: Artificial Glaciers as a Focus of Environmental Knowledge and Development Interventions, in: Ethnic and Cultural Dimensions of Knowledge, edited by Meusburger, P., Freytag, T., and Suarsana, L., Knowledge and Space, pp. 191–209, Springer International Publishing, Cham, https://doi.org/10.1007/978-3-319-21900-4_9, 2016.

Nüsser, M., Dame, J., Kraus, B., Baghel, R., and Schmidt, S.: Socio-Hydrology of Artificial Glaciers in Ladakh, India: Assessing Adaptive Strategies in a Changing Cryosphere, Regional Environmental Change, https://doi.org/10.1007/s10113-018-1372-0, 2019.

Oerlemans, J. and Knap, W. H.: A 1 Year Record of Global Radiation and Albedo in the Ablation Zone of Morteratschgletscher, Switzerland, Journal of Glaciology, 44, 231–238, https://doi.org/10.3189/S0022143000002574, 1998.

Oerlemans, J., Balasubramanian, S., Clavuot, C., and Keller, F.: Brief Communication: Growth and Decay of an Ice Stupa in Alpine Conditions – a Simple Model Driven by Energy-Flux Observations over a Glacier Surface, The Cryosphere, 15, 3007–3012, https://doi.org/10.5194/tc-15-3007-2021, 2021.

Palmer, L.: Storing Frozen Water to Adapt to Climate Change, Nature Climate Change, 12, 115–117, https://doi.org/10.1038/s41558-021-01260-x, 2022.

Reuters: Conservationists in Chile Aim to Freeze Water in Man-Made Glaciers, Reuters, 2021.

Schmidt, L. S., Aðalgeirsdóttir, G., Guðmundsson, S., Langen, P. L., Pálsson, F., Mottram, R., Gascoin, S., and Björnsson, H.: The Importance of Accurate Glacier Albedo for Estimates of Surface Mass Balance on Vatnajökull: Evaluating the Surface Energy Budget in a Regional Climate Model with Automatic Weather Station Observations, The Cryosphere, 11, 1665–1684, https://doi.org/10.5194/tc-11-1665-2017, 2017.

ShiChang, TanGuang, G., ShiQiao, Z. G. Z., and Kang: Response of Zhadang Glacier Runoff in Nam Co Basin, Tibet, to Changes in Air Temperature and Precipitation Form, Chinese Science Bulletin, 55, 2103–2110, https://doi.org/10.1007/s11434-010-3290-5, 2010.

Steiner, J. F., Pellicciotti, F., Buri, P., Miles, E. S., W, T. D. I. W., and Reid: Modelling Ice-Cliff Backwasting on a Debris-Covered Glacier in the Nepalese Himalaya, Journal of Glaciology, 61, 889–907, https://doi.org/10.3189/2015JoG14J194, 2015.

Tveiten, I.: Glacier Growing - A Local Response to Water Scarcity in Baltistan and Gilgit, Pakistan, Ph.D. thesis, 2007.

Vince, G.: Glacier Man, Science, 326, 659–661, https://doi.org/10.1126/science.326_659, 2009.

Vincent, S.: Energy and Climate Change in Cold Regions of Asia, 2009.

Wangchuk, S.: Ice Stupa Competition, https://tribal.nic.in/IceStupa.aspx, 2020.

Zolles, T., Maussion, F., Galos, S. P., Gurgiser, W., and Nicholson, L.: Robust Uncertainty Assessment of the Spatio-Temporal Transferability of Glacier Mass and Energy Balance Models, The Cryosphere, 13, 469–489, https://doi.org/10.5194/tc-13-469-2019, 2019.